International Journal of Hydrogen Energy 83 (2024) 387–395

Contents lists available at ScienceDirect

International Journal of Hydrogen Energy

journal homepage: www.elsevier.com/locate/he

The role of Na decoration on the hydrogen adsorption on coronene: A combined experimental and computational study

Esther García-Arroyo [a], Anna Maria Reider [b], Siegfried Kollotzek [b], Florian Foitzik [b], José Campos-Martínez [a], Massimiliano Bartolomei [a], Fernando Pirani [c], Marta I. Hernández [a,*], Massimo Mella [d,*], Paul Scheier [b,*]

[a] Instituto de Física Fundamental, Consejo Superior de Investigaciones Cianti,ficas (IFF-CSIC), Serrano 123, Madrid, E-28006, Spain
[b] Institut für Ionen Physik und Angewandte Physik, Universität Innsbruck, Technikerstr. 25, Innsbruck, A-6020, Austria
[c] Dipartimento di Chimica, Biologia e Biotecnologie, Università di Perugia, via Elce di Sotto 8, Perugia, 06123, Italy
[d] Dipartimento di Scienza ed Alta Tecnologia, Università degli Studi dell'Insubria, via Valleggio 11, Como, 22100, Italy

ARTICLE INFO

Keywords:
Hydrogen adsorption and storage
Helium nanodroplets experiments
Polycyclic aromatic hydrocarbons
Alkali atom decoration

ABSTRACT

Functionalizing carbon-based materials with metal atoms has been proposed as an effective method to enhance the adsorption of hydrogen molecules on these substrates, thereby developing new useful systems for hydrogen storage. In this work, we investigate both experimentally and theoretically the role of sodium atom decoration on hydrogen attachment to coronene, a polycyclic aromatic hydrocarbon considered the smallest prototype of graphene. In the experiments, multiply charged helium nanodroplets are produced and exposed to sodium, coronene and hydrogen vapors, leading to the formation, within equal conditions, of clusters of hydrogen molecules surrounding bare and sodium-decorated protonated coronene, $[H\text{-coronene}]^+$ and $[H\text{-coronene-Na}]^+$, respectively, whose abundances are accurately measured via mass spectrometry. These clusters are studied computationally by means of quantum Monte Carlo methods, using analytical representations of the H_2-substrate interaction potentials based on high-level electronic structure calculations. It is found that the number of H_2 molecules attached to both $[H\text{-coronene}]^+$ and $[H\text{-coronene-Na}]^+$ decreases as the evaporation pressure in the H_2 chamber increases; however, the Na-decorated support retains a considerably larger number of molecules than the undecorated one, which is related to the higher evaporation energies of H_2 molecules attached to the decorated support. In addition, most of the anomalies observed in the distributions of ion abundances vs. the number of hydrogen molecules have been identified in the theory as particularly stable clusters. For the Na-decorated substrate, it is found that clusters formed by four H_2 molecules surrounding Na are very stable and that with the addition of two more molecules, the alkali atom becomes "solvated".

1. Introduction

Adsorption of molecular hydrogen to carbon-based materials has been proposed as a safe and efficient method of hydrogen storage, a goal that is a key step in the development of new environmentally friendly technologies that use this element as an energy carrier [1–8]. These materials, such as graphene, are in principle very appealing to these purposes because of their light weight, large surface area, great stability and robustness [9–12]. However, as hydrogen molecules interact with them via weak van der Waals forces (with binding energies in the range of a few tens of meV [13]), hydrogen adsorption only occurs efficiently at rather low temperatures.

The functionalization of carbon materials with metals gives rise to an enhancement of the hydrogen binding energies, eventually improving the adsorption properties. Focusing on their decoration with neutral alkali metals, this enhancement stems from the partial donation of the metal valence electron to the carbon support, so that the alkali atom acquires a partial positive charge when bound to the substrate [14–16]. It is worth noting that similar binding properties have been found in the interaction of alkali *cations* to carbonaceous materials [17,18]. Hydrogen molecules close to these metals become polarized and their bonding to them – besides the ubiquitous van der Waals forces – is due to the interaction of the charge with the induced dipole and with the permanent quadrupole of hydrogen, pretty similar to the interactions between these particles in the gas phase [19]. These non-covalent forces are more attractive than pure van der Waals ones and have the peculiarity that the ionic center can become surrounded by various hydrogen molecules. These properties lead to enhanced gravimetric and

* Corresponding authors.
E-mail addresses: marta@iff.csic.es (M.I. Hernández), massimo.mella@uninsubria.it (M. Mella), Paul.Scheier@uibk.ac.at (P. Scheier).

https://doi.org/10.1016/j.ijhydene.2024.07.425
Received 22 May 2024; Received in revised form 8 July 2024; Accepted 28 July 2024
Available online 12 August 2024

volumetric densities and move the temperature range for a reversible adsorption/desorption process to higher values [10,14,20]. This work concerns these interactions, still falling within the category of physical adsorption – the hydrogen molecule retains its identity –, as opposed to chemisorption, not considered here, where the molecule breaks and its atoms covalently attach to the substrate [21–23].

This physical adsorption of hydrogen on carbonaceous materials (bare or decorated with alkali metals) has been the subject of numerous theoretical studies [9,14,15,20,24–31], however, experimental studies have been scarcer [32–37]. Among the different carbon-based materials, considerable attention has been devoted to polycyclic aromatic hydrocarbons (PAHs), as prototypes of extended materials or as alternative storage systems [13,18,37–44]. Adsorption of hydrogen to PAHs is also a subject of great interest in astrochemistry [45]. Very recently, some of us have reported a joint experimental and theoretical investigation where Na-decorated naphthalene, as a hydrogen adsorbent, was compared to bare naphthalene [46]. Calculations and measurements confirmed an enhancement in H_2 adsorption for the decorated substrate, and agree with the finding of special stability of clusters formed by four H_2 molecules surrounding the alkali atom, with some minor discrepancies about other specially stable structures (magic numbers). In addition, larger Na-decorated PAHs were studied using more approximated calculations but without the experimental counterpart.

In this work, we focus both experimentally and computationally, on the adsorption of hydrogen on bare and sodium-decorated coronene, a PAH commonly considered the smallest graphene prototype [47,48]. In the experiments, complexes of hydrogen molecules coating protonated coronene (coro), both bare, $(H_2)_n$[H-coro]$^+$, and sodium-decorated, $(H_2)_n$[H-coro-Na]$^+$, are abundantly produced inside ultracold helium nanodroplets and, after their passage through an evaporative cell, populations of these clusters are accurately measured, enabling the identification of the most stable complexes. Interestingly, both bare and Na-decorated substrates are produced and studied under the same experimental conditions, allowing us to explore in a direct and unbiased manner the role of sodium decoration. These results are compared with quantum Monte Carlo calculations of the clusters' ground state energies and structures, obtained with the use of force fields carefully parametrized on high-level electronic structure calculations of the H_2-substrate interaction. These calculations provide accurate determinations of nuclear quantum effects – such as the zero-point energy of the adsorbed molecules – which are generally quite important for this lightweight species [9,13,49,50] but are not usually considered in works that only focus on the electronic structure of these kinds of systems.

The paper is organized as follows: experimental and computational methods are presented in Sections 2 and 3, respectively. In Section 4, the results of the joint investigation on bare and Na-decorated coronene are reported and discussed. Finally, concluding remarks are given in Section 5.

2. Experimental method

This section gives an overview of the experimental part of this work, the details of the setup and methods can be found in the literature [51,52]. A schematic sketch of the apparatus can be seen in Fig. 1.

Superfluid helium nanodroplets (HNDs) are formed via supersonic expansion of pressurized (22 bar), and pre-cooled (8.8 K) helium gas (Messer, purity 99.9999%) through a pinhole nozzle (5 μm diameter) into ultra-high vacuum. The HNDs are ionized via electron impact, with the ion source operated at an electron energy of 40 eV and electron current of 340 μA to generate multiply charged droplets. Hydrogen gas that is introduced into a differentially pumped RF-hexapole further downstream the experiment at relatively high pressures (between 1.69×10^{-3} and 3.72×10^{-3} mbar) is reaching the ion source chamber and H_2 is likely the first dopant to be picked up by the HNDs. Charge transfer

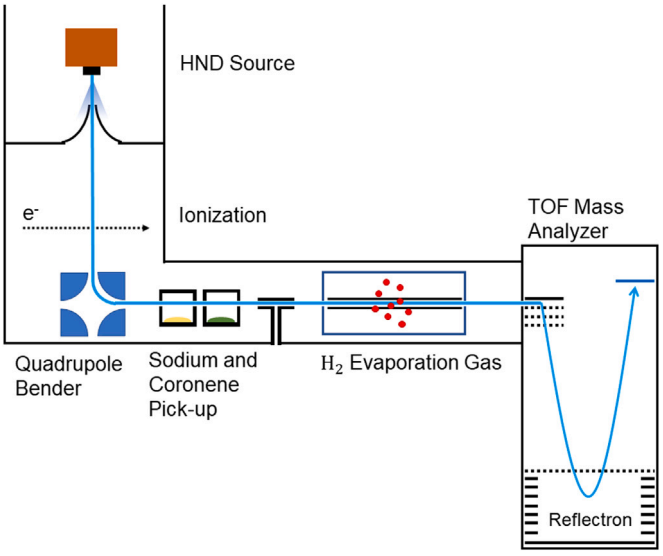

Fig. 1. Superfluid helium nanodroplets (HNDs) are produced in the cluster source and multiply charged via electron impact. Due to the back-flow of the hydrogen evaporation gas into this chamber, H_2 molecules are doped into the HNDs before a quadrupole bender filters the droplet beam for one mass-per-charge ratio. These size-selected HNDs then traverse through pick-up cells with sodium and coronene vapor. The dopant ions are liberated from the He matrix and tagged with H_2 through collisions with hydrogen gas at varying pressures. The resulting ions are detected in a reflectron time-of-flight mass spectrometer (TOF Mass Analyzer).

from initially formed He^+ will ionize hydrogen and additional pickup of H_2 molecules will form $(H_2)_nH_3^+$ ionic cores close to the surface of the droplets. A subsequent quadrupole bender allows the selection of the charged droplets by their mass-per-charge ratio, resulting in the current experiment in HNDs consisting of approximately 7.5×10^4 He atoms per charge and an approximate kinetic energy of 400 eV. Coronene powder (SigmaAldrich, 99% purity) and sodium (SigmaAldrich, 99.95%) are evaporated in resistively heated ovens. The similar evaporation pressures of the dopants, as well as the geometry of the ovens, lead to a mixture of the gas phases, resulting in simultaneous pick-up of the two substances into the HNDs. Ion-induced dipole interaction then attracts coronene and sodium towards the $(H_2)_nH_3^+$ charge centers, where charge transfer leads to the formation of Na^+ or proton transfer to [H-coro]$^+$ and subsequently picked up dopants attach to the ionic cores forming [H-coro$_m$-Na$_k$]$^+$ and [coro$_m$-Na$_k$]$^+$ complexes, respectively. The corresponding binding energy is transferred to the surrounding He matrix, causing evaporation of about 1600 He atoms per eV and the stabilization of the clusters. In the RF hexapole cell, collisions with H_2 molecules lead to the shrinking of the HNDs and solvation of the dopant ions by hydrogen. Due to the increasing Coulomb repulsion, this shrinking causes the sequential ejection of hydrogen-solvated cluster ions. Typically, the removal of 10^5 He atoms is necessary to eject each ionic core [53]. Subsequent collisions of the ejected ionic complexes with hydrogen gas reduce the number of H_2 molecules attached to a favorable value. Hence, high hydrogen pressures in the cell result in fewer H_2 molecules solvating the ejected ions, which are then analyzed in a time-of-flight mass spectrometer. Exemplary mass spectra are shown in Fig. 2. Due to the conditions during the ionization process and the later pick-up of coronene and Na, the protonated substrates [H-coro]$^+$ and [H-coro-Na]$^+$ become most abundant and are hence the focus of this work.

3. Theoretical method

We have performed Diffusion Monte Carlo calculations of the ground state energies and distributions of the clusters $(H_2)_n$[H-coro]$^+$ and

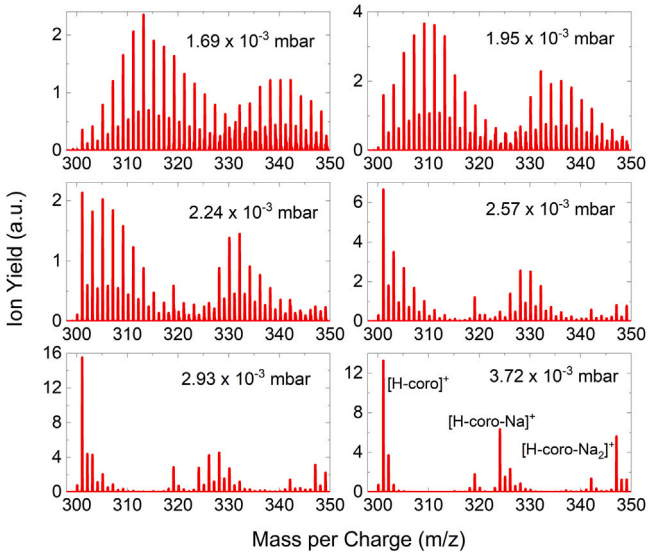

Fig. 2. Mass spectra resulting from different H_2 pressures in the evaporation cell where a higher hydrogen pressure leads to lower hydrogen solvation of the clusters. The absolute ion yields are given to compare the differing levels of the signal.

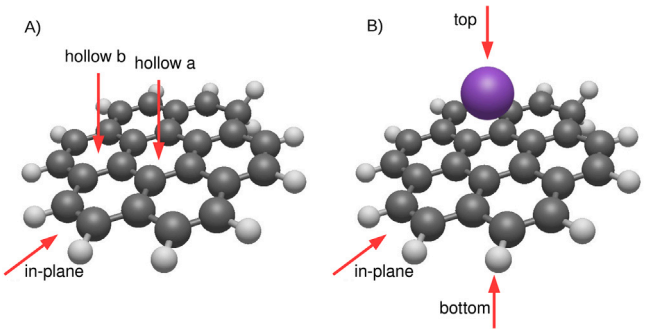

Fig. 3. Left panel A: $[H\text{-coro}]^+$ substrate, with red arrows indicating the different approach directions of the center of mass of the H_2 molecule. **hollow a** is the direction perpendicular to the coronene plane towards its geometrical center, **hollow b** is also perpendicular but towards the center of a peripheral hexagon and **in-plane** indicates the direction along the molecule plane towards the middle of an outer C–C bond and the center of the coronene. Right panel B: just like panel A, but for $[H\text{-coro-Na}]^+$. **top** is the direction perpendicular to the coronene plane towards its geometrical center from the face with sodium, **bottom** is also perpendicular, along the top direction, but from the bare face and **in-plane** indicates the direction along the molecule plane exactly as in panel A. (For interpretation of the references to color in this figure legend, the reader is referred to the web version of this article.)

$(H_2)_n[H\text{-coro-Na}]^+$. In the present model, we treat the substrates as rigid molecules and the hydrogen molecules, as pseudoatoms, i.e., only the motion of the centers of mass of the H_2 molecules is explicitly considered in the simulations. This pseudoatom approximation has been shown to be rather appropriate for the description of the evaporation energies of related systems, such as the attachment of hydrogen to Na^+ or to Na-decorated naphthalene [46,54]. We firstly present the electronic structure calculations of the H_2-substrate interactions together with their analytical representation within the adopted model, followed by a description of the Diffusion Monte Carlo calculations of the clusters ground states.

3.1. Electronic structure calculations

Electronic structure calculations have been carried out to obtain reference energy potentials for the interaction between the H_2 molecule and the Na-decorated and bare protonated coronene cations, $[H\text{-coro-Na}]^+$ and $[H\text{-coro}]^+$. In these calculations the monomers have been considered as rigid rotors. The decorated and bare $[H\text{-coro}]^+$ geometries have been optimized in the same way as it was previously done on naphthalene [46], while the interatomic distance of the H_2 molecule has been fixed to 0.767 Å, corresponding to the averaged value in the ground vibrational state. For the case of the decorated coronene, it is found that the distance of the sodium atom to the coronene plane is 2.33 Å. Moreover, the binding energy obtained by subtracting the sodium cation from the neutral coronene is about 1.5 eV, indicating that the decorated coronene complex is indeed strongly bound and that it can be safely treated as a rigid body.

In the calculations of the intermolecular interaction energies, three different approach directions of the H_2 center of mass towards the decorated and bare protonated coronene have been considered, as shown in Fig. 3. For each approach direction, three different limiting orientations of the H_2 molecular axis have also been taken into account, which correspond to two parallel and one perpendicular orientation with respect to the coronene plane. The different interaction potentials for each approach have been calculated at the Kohn–Sham Density Functional Theory (DFT) level using a spin-restricted formalism, with the B3LYP [55] exchange–correlation functional together with the D3 dispersion correction [56] and a triple-zeta (VTZ) [57] basis set. The only exception corresponds to the top approach in the case of $[H\text{-coro-Na}]^+$, for which we have followed a different strategy based on benchmark results obtained for the H_2 interaction with Na-decorated naphthalene [46] (see Figure S1 in the Supplementary Information). In this case, we have extrapolated the interaction energies to obtain the values corresponding to the complete basis set (CBS) [58,59] by combining the results obtained with the spin-component scaled second-order Møller–Plesset (MP2-SCS) [60] perturbation theory with those at MP2 and Hartree–Fock levels for two different basis sets: augmented double-zeta [57] (AVDZ) and augmented triple-zeta (AVTZ). All the interaction energies have been corrected for the basis set superposition error (BSSE) by using the counterpoise method of Boys and Bernardi [61].

All the calculations have been computed using the Molpro 2022.2 software package [62]. The computed interaction energies are shown as black points in Fig. 4 and correspond, for each approach direction, to values averaged over the three different considered orientations of the H_2 molecule. Such values represent a good estimation of the pseudoatom approximation for H_2.

3.2. Interaction potential analytical representation

The interaction potential between the H_2 molecule – as a pseudoatom – and decorated and undecorated coronene is expressed by a sum of pairwise contributions for each H_2-atom interacting pair:

$$V = \sum_i V^i, \tag{1}$$

where i sums over all atoms in the coronene substrates. Each of these V_i terms is given by the Improved Lennard-Jones (ILJ) [63] formulation:

$$V^i = \varepsilon \left[\frac{m}{n(r)-m} \left(\frac{r_m}{r}\right)^{n(r)} - \frac{n(r)}{n(r)-m} \left(\frac{r_m}{r}\right)^{m} \right], \tag{2}$$

where ε and r_m represent the well depth and equilibrium distance of the pair interaction, respectively, $n(r)$ is expressed like $n(r) = \beta + 4.0\,(r/r_m)^2$ where β is a parameter defining the shape and stiffness of the potential. Finally, m is a parameter whose value is 6 for neutral–neutral interactions and 4 for ion-neutral ones.

As the pair interaction between H_2 molecules is considered as the one for pseudoatoms, it can be expressed again using the formulation in Eq. (2).

The used ILJ parameters for the different H_2-atom and H_2–H_2 molecules interaction pairs are given in Table 1.

The H_2–C, H_2–H and H_2–Na parameters have been optimized by exploiting the comparison with the electronic structure results and the

Table 1
ILJ optimized parameters for the H_2–C, H_2–H and H_2–Na contributions involved in the interaction between H_2 and coronene. The corresponding parameters for the H_2–H_2 interaction are also reported. In this model, H_2 is described as a point-like particle (pseudoatom). ϵ is in meV, r_m is in Å and β and m are dimensionless.

	ϵ	r_m	β	m
H_2–C	4.30	3.45	7.0	6
H_2–H	2.15	3.17	6.1	6
H_2–Na	52.0	2.75	4.6	4
H_2–H_2 [64]	3.07	3.47	7.0	6

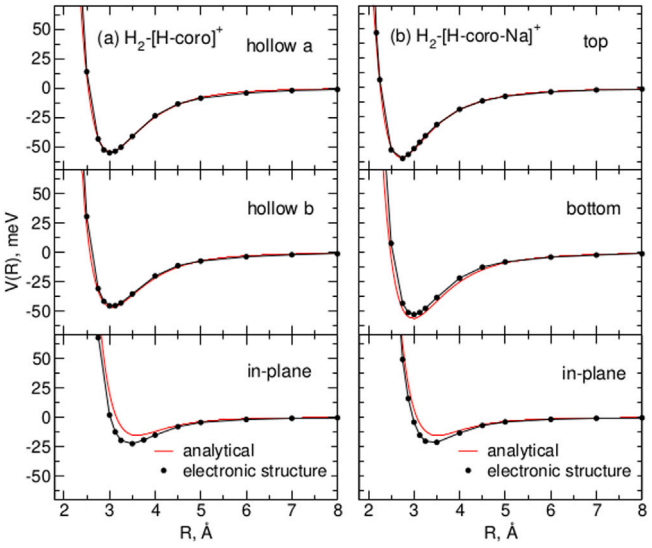

Fig. 4. Interaction energy potentials for H_2 approaching $[H\text{-coro}]^+$ (left panel a) and $[H\text{-coro-Na}]^+$ (right panel b) along the directions illustrated in Fig. 3. The black points correspond to the electronic structure results while the red lines to the obtained analytical potentials. (For interpretation of the references to color in this figure legend, the reader is referred to the web version of this article.)

final estimated analytical profiles are shown as red solid lines in Fig. 4, where a good agreement can be appreciated.

3.3. Diffusion Monte Carlo simulations

To study the energetics associated with the adsorption of H_2 molecules on the decorated and undecorated coronene, we have used Diffusion Monte Carlo (DMC), a technique that allows, in principle, to exactly solve the Schrödinger equation for molecular clusters by sampling a density of configurations proportional to the ground state wave function, ψ_0 (e.g. see Refs. [65–67]). In this respect, it can both determine the ground state energy of clusters as well as the relative molecular distribution.

DMC works projecting an initial distribution of configurations in imaginary time applying diffusion and branching steps to propagate the latter [68] for the system under study. While the diffusion step randomly displaces configurations accordingly with a Gaussian kernel of width depending on the molecular masses and integration time-step, the branching algorithm changes the number of configurations accordingly to a computed weight; the latter is defined based on the difference between the value of the potential energy for each configuration and a reference energy appropriately selected to conserve the number of configurations. Once the weights are defined, system replicas are killed or duplicated based on a random selection game, where the reference energy is adjusted for the next step [69]. After a steady state is reached, the distribution of points representing the ground state wave function can be used to estimate the system ground state energy by computing the potential energy average [70]. In order to minimize integration timestep errors and the bias due to the finite population size, we have used a timestep of 100 a.u. and a number of walkers that oscillates around 650.

The ground energies and configuration distributions for both bare and Na-decorated coronene systems have been calculated up to a number of 14 hydrogen molecules; the results are described in the following sections.

4. Results and discussion

The experimental data of this study were analyzed via the home-built software IsotopeFit [71] to determine the exact yield of the hydrogen solvation within the $(H_2)_n[H\text{-coro}]^+$ and $(H_2)_n[H\text{-coro-Na}]^+$ series, respectively. From the mass spectra shown in Fig. 2 the software identifies the correct cluster size by considering the isotopic pattern of coronene, potential isobaric impurities (such as clusters with helium attachment or those with water picked up from the residual gas) and the background signal from neighboring ion peaks. The resulting ion yields in Fig. 5 depict the differences in $(H_2)_n$ attachment as a function of the number of hydrogen molecules, n, to the coronene cluster with or without sodium at different evaporation pressures. For each pressure, the yields of each $(H_2)_n[H\text{-coro}]^+$ and $(H_2)_n[H\text{-coro-Na}]^+$ series are normalized by the total ion yields of all protonated substrates containing no Na, $\sum_n H_{2n}[H\text{-coro}]$, or one Na, $\sum_n H_{2n}[H\text{-coro-Na}]$, respectively. This corrects the effects of the Poisson statistics in the pick-up process and consequent cluster formation. During this process, it is more probable to form undecorated species in comparison to complexes containing one or more Na atoms, as evident in the mass spectra of Fig. 2. At all pressures in Fig. 5 it becomes apparent that with increasing cluster size of $(H_2)_n$, the sodium-decorated complexes are more stable and hence show higher yields compared to the $(H_2)_n[H\text{-coro}]^+$ substrate. Additionally, it is noticeable that at lower H_2 evaporation pressures (1.69×10^{-3}–1.95×10^{-3} mbar), the distributions of the $(H_2)_n$ attachment is similar for the support with and without Na. However, at increasing pressures, the undecorated $[H\text{-coro}]^+$ support loses the amount of attached H_2 molecules considerably faster than the Na decorated counterpart. This indicates that the Na decorated clusters are more resilient against increasing collision frequencies, as the H_2 molecules become more tightly bound compared to those on $(H_2)_n[H\text{-coro}]^+$.

At this point it is worth noting the differences between the present experiment and those aimed at studying hydrogen storage at conditions within the requirements of the U. S. Department of Energy (DOE) [72]. In particular, typical pressures of this experiment (10^{-3} mbar) are several orders of magnitude smaller than the required pressures in a storage system (5–12 bars). In the present case, complex ions cross the H_2 evaporation chamber at a rather high velocity, determined by the difference of the electrostatic potential of the electron ionization region and the field axis of the RF-hexapole guide. The pressure in the cell determines the number of collisions the ions have with a stagnant H_2 gas target at a collision energy that is mostly determined by the kinetic energy of the ions. On the other hand, in a storage system, substrate molecules are embedded in a hydrogen gas at a pressure of several bars, which provides many more collisions, however, at a much lower collision energy, in this case solely determined by the temperature of the gas.

The slower(faster) loss of H_2 molecules attached to the metal decorated(undecorated) carbonaceous surface as the pressure of the collision gas increases (Fig. 5) is an effect that becomes clearly visible in Fig. 6, where the percentage of adsorption to either the decorated or the bare substrate is shown depending on the corresponding evaporation pressure. This highlights the efficiency of the H_2 attachment on $[H\text{-coro-Na}]^+$ at increasing pressures and suggests an increase of the evaporation energies of the H_2 molecules on the sodium-decorated clusters. In other words, when more H_2 molecules are removed at increasing pressures, the substrate with the alkali atom retains more molecules and therefore adsorbs a larger percentage of hydrogen.

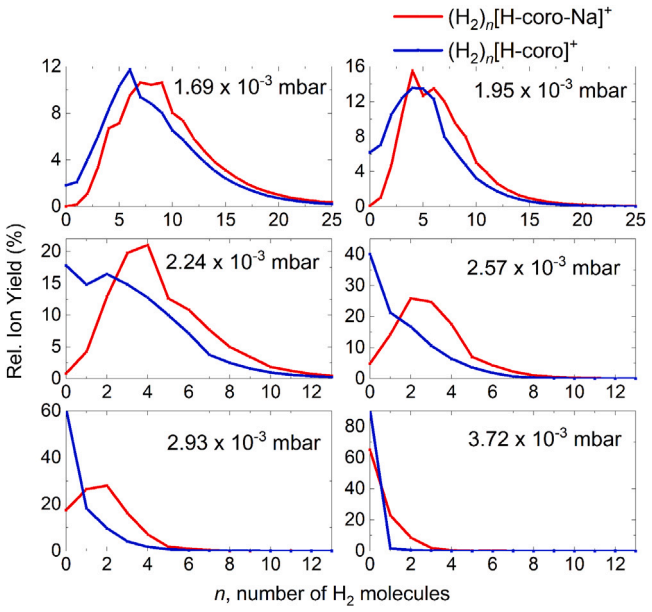

Fig. 5. Relative ion yield of the number of adsorbed H_2 molecules on each substrate. The normalization corresponds to the total ion yield of the $(H_2)_n$[H-coro]$^+$ or $(H_2)_n$[H-coro-Na]$^+$ series at each evaporation pressure.

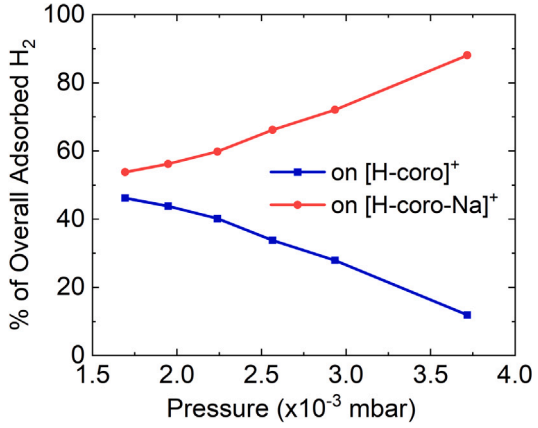

Fig. 6. Pressure dependence of the percentage distribution of adsorbed H_2 molecules on [H-Coro]$^+$ and [H-Coro-Na]$^+$ substrates within one experimental run.

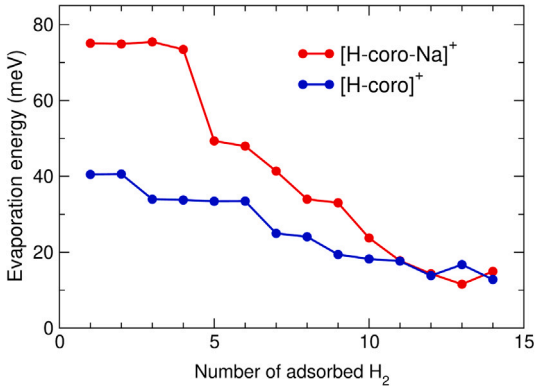

Fig. 7. Evaporation energies, $\Delta E_n = E_{n-1} - E_n$ (meV), as functions of the number of H_2 molecules adsorbed on the decorated (in red) and bare (in blue) substrates. (For interpretation of the references to color in this figure legend, the reader is referred to the web version of this article.)

On the theoretical side, we have obtained the ground state energies, E_n, of the clusters formed by n = 1–14 hydrogen molecules attached to [H-coro-Na]$^+$ and [H-coro]$^+$. A good measure of the stability of these complexes is given by the evaporation energy $\Delta E_n = E_{n-1} - E_n$, which is the energy required to adiabatically remove the most weakly bound H_2 molecule from a cluster with n molecules. In Fig. 7, these energies are presented as functions of n for the two substrates studied. It is clear that they are larger for the alkali-decorated support, particularly for the first four attached molecules. This is due to the stronger binding of H_2 to the Na atom, as discussed in more detail below. For $n > 10$, the evaporation energies become smaller and almost equal for the two substrates, suggesting that at these sizes the alkali atom no longer has a dominant effect on the cluster stability. These features can be qualitatively related to the observed relative ion yields of Fig. 5 and the subsequent percentage of H_2 adsorption of Fig. 6. Indeed, for pressures up to 2.24×10^{-3} mbar, cluster abundances extend up to more than ten H_2 molecules (Fig. 5) and from Fig. 6 it is seen that they adsorb to either support in a similar proportion (50 ± 10%). For higher pressures, species with more than ten molecules attached are no longer observed and there is an increasing trend for H_2 adsorption to the Na-decorated substrate (reaching 90% for the highest pressure), a feature that we interpret as a consequence of the larger evaporation energies of the decorated substrate for these cluster sizes.

The relative ion yields of Fig. 5 generally follow an expected Poisson distribution [51] with various anomalies (locally larger abundances) which suggest that some cluster sizes are relatively more stable than their neighbors. For instance, the $(H_2)_4$[H-coro-Na]$^+$ cluster seems to be more abundant than the n = 3 and 5 clusters for most evaporation pressures. In the calculations, the n = 4 Na-decorated complex appears to be particularly stable, due to its large evaporation energy in comparison to the n = 5 one (Fig. 7). Recent DFT calculations also found a special stability for four H_2 molecules attached to [coro-Na]$^+$[44]. To establish a quantitative determination of these anomalies and its relationship with the computed evaporation energies, we have followed the approach originally proposed in Ref. [73], also recently applied on $(H_2)_n$Na$^+$ and $(H_2)_n$[H-naphthalene-Na]$^+$ systems [46,74]. This model assumes that the experimental abundance I_n and the corresponding evaporation energy ΔE_n are related as

$$\frac{I_n}{I_{av}} \approx \frac{\Delta E_n}{\Delta E_{av}}, \tag{3}$$

where I_{av} and ΔE_{av} are local averages of I_n and ΔE_n. As discussed in detail in Refs. [75,76], Eq. (3) applies when the observed cluster ions are the unimolecular fragments of larger precursors and, in addition, their internal vibrational modes are not excited at the relevant temperatures. These conditions are met in the present experiment. In Figs. 8 and 9, we present a comparison between the left- and right-hand sides of Eq. (3) as functions of n, for substrates [H-coro-Na]$^+$ and [H-coro]$^+$, respectively. Averages I_{av} and ΔE_{av} over neighboring cluster sizes were obtained using a normalized Gaussian distribution [77] centered at each cluster size and with a standard deviation σ = 1. The experimental ratios of Figs. 8 and 9 (upper panels) are shown for evaporation pressures from 1.69×10^{-3} to 2.93×10^{-3} mbar (for the highest pressures the set of ratios shown is reduced to the range with non-negligible intensities associated). It is worth noticing that the maxima obtained in I_n/I_{av} for various values of n are almost independent of the pressure. In other words, they are not due to accidental maxima in the size distribution of ion abundances but rather can be associated with magic numbers (this statement does not apply as much to the highest pressures, where the abundances distributions are narrower and the ratios become more sensitive to them).

Moving to the comparison of $\Delta E_n/\Delta E_{av}$ with I_n/I_{av} for [H-coro-Na]$^+$, in Fig. 8, it can be seen that a good agreement has been achieved. Specifically, both intensity and evaporation energy ratios indicate that the n = 4 and n = 9 clusters are magic numbers as well as, to a lesser extent, the n = 6 and 7. A minor discrepancy is related to larger cluster

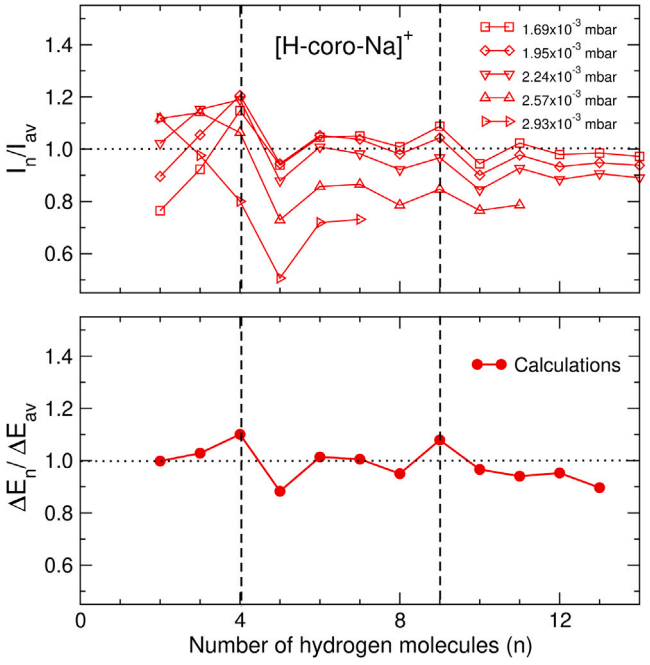

Fig. 8. Upper panel: ratios between the observed ion abundances and their local averages vs. n, the number of H_2 molecules adsorbed on $[H\text{-coro-Na}]^+$, for various pressures in the evaporation cell. Lower panel: ratios between the calculated evaporation energies and their local averages vs. n for the same substrate. The resemblance between the experimental and theoretical ratios implies that Eq. (3) holds reasonably well. Cluster sizes for which the ratios reach a local maximum indicate that the corresponding clusters are especially stable (magic numbers). The two most evident magic numbers are indicated by vertical dashed lines. See text for discussion.

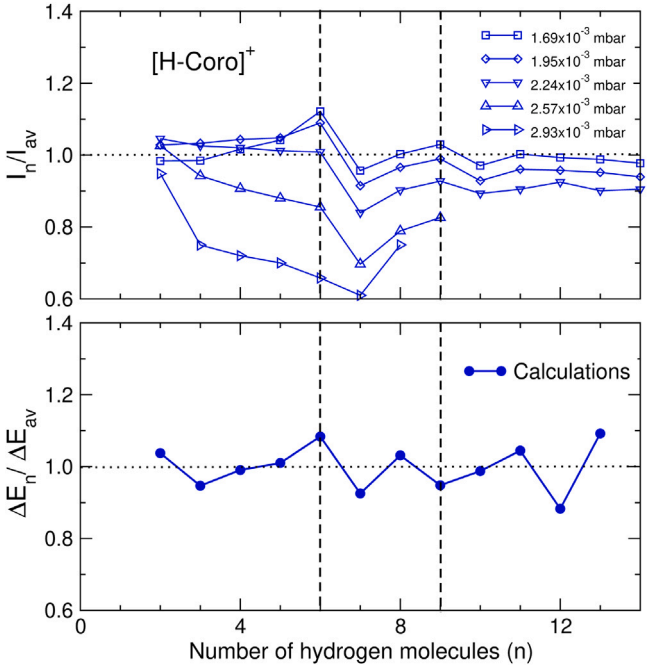

Fig. 9. Same as in Fig. 8, for the adsorption of H_2 molecules on $[H\text{-coro}]^+$. The two most evident magic numbers, experimentally observed, are indicated by vertical dashed lines.

sizes since the next magic number is $n = 11$ in the experiments, but $n = 12$ in the calculations. Regarding the bare substrate, in Fig. 9, it can be seen that both theory and experiment agree that $n = 6$ is a quite stable complex as well as, to a minor degree, $n = 11$. The cluster formed with two molecules attached is also found to be quite stable from the calculations, the finding being in reasonable agreement with the behavior of the experimental ratios at the highest pressures. There is no agreement, however, in the next magic number, which is $n = 9$ in the experiment but $n = 8$ in the theory. Reasons for the mentioned discrepancies could be related to some simplifying assumptions of the theoretical model, such as the description of the H_2 molecules as pseudoatoms. Despite it has been shown that this approximation works well for related systems [46], a more accurate description of these molecules as rigid rotors could modify the relative stability of some cluster sizes, an issue worth investigating in the future.

To understand the stability patterns of these systems, we have examined the structures of n H_2 molecules adsorbed on $[H\text{-coro-Na}]^+$ and $[H\text{-coro}]^+$, obtained from the DMC probability distributions. For the sodium-decorated support, the first four molecules are successively placed around Na and above the coronene molecule. Probability distributions of the magic number $n = 4$ are shown in Fig. 10. It can be seen that they extend about 3.2 Å above the coronene plane (Fig. 10.a), forming a ring around the Na atom (Fig. 10.b, notice a somewhat larger probability density on top of the centers of the peripheral hexagonal rings of coronene). For $n = 5$, the molecules also arrange along a ring around sodium; the reason that the $n = 5$ cluster is less stable than the $n = 4$ one must lie in an increase of the repulsion between the hydrogen molecules, which nevertheless are confined around Na due to the attraction exerted by this atom (i.e., electrostriction effect [64,78]). Then, the sixth molecule is placed on top of Na, six being the maximum number of molecules closely attached to Na, in other words, the number of molecules that solvate the alkali atom. The following three molecules become placed on the side of $[H\text{-coro-Na}]^+$ without Na. Using the notation (n_a, n_b), where n_a and n_b indicate the number of molecules on the sides without and with sodium, respectively, the $n = 7$–9 clusters can be assigned to (1,6), (2,6) and (3,6) arrangements, respectively. The probability density for $n = 9$ (3,6), along the direction perpendicular to coronene, is depicted in Fig. 10.a. The special stability of this cluster size can be understood from the solvation of sodium with six molecules on the side with Na (Fig. 10.d) and, on the opposite side, from a maximization of the attractive interactions of the three H_2 molecules with the support and among themselves (Fig. 10.c). Furthermore, it is worth noticing that the three H_2 molecules of Fig. 10.c are rather delocalized, in contrast to the six ones of the decorated side (Fig. 10.d); analogous features of localization vs. delocalization have been found and discussed for the distributions of rare gas atoms [79] and H_2[13] adsorbed to coronene. Finally, the structures found for $n = 10$–14 correspond to (n_a, n_b)= (4,6), (5,6), (5,7), (5,8) and (6,8) arrangements, respectively.

For the bare substrate, $[H\text{-coro}]^+$, H_2 molecules tend to distribute equally on both sides of the molecule, that is, from $n = 1$ to 6, the most stable arrangements are (n_a, n_b)= (1,0), (1,1), (2,1), (2,2), (3,2) and (3,3), respectively. The most stable cluster, as found both in the calculations and in the experiment, is the one having six H_2 molecules adsorbed. The special stability of the $n = 6$ cluster can be understood as an optimization of the attractive interactions of the three H_2 molecules that are on each side of the support (as in the case of the side without Na of $(H_2)_9[H\text{-Coro-Na}]^+$, discussed above). In this point, it is worth mentioning that this magic number has already been identified in related experiments [40] as well as in computational studies of the adsorption of hydrogen to neutral [13] and cationic [46,50] coronene. For larger clusters, $n = 7$–14, the most stable structures correspond to arrangements (n_a, n_b) = (4,3), (4,4), (5,4), (5,5), (6,5), (7,5), (7,6) and (8,6).

As discussed above, the kind of experiments here reported are quite different from set-ups to measure hydrogen storage at pressures and temperatures typical of the desired applications. For this reason, it is not straightforward to extrapolate present results to these situations. Nevertheless, we have estimated the gravimetric capacity of

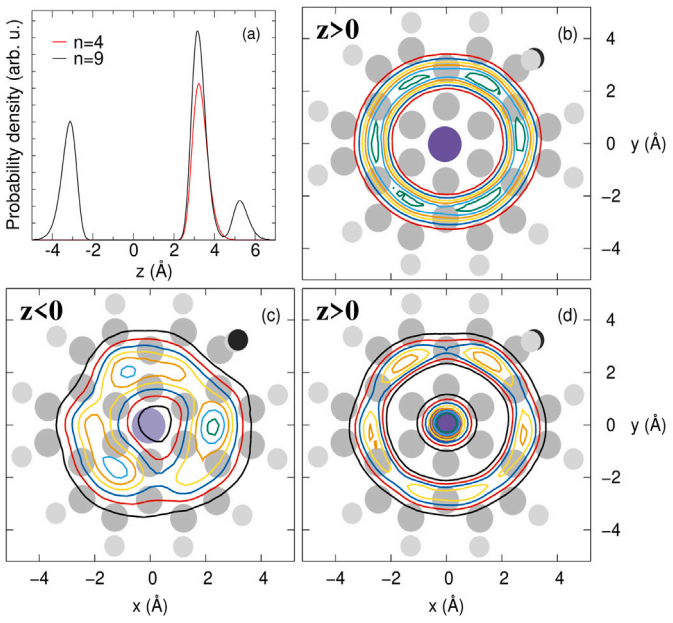

Fig. 10. (a) Probability distributions along the axis perpendicular to coronene (z) of $n = 4$ (in red) and $n = 9$ (in black) H_2 molecules attached to $[H\text{-coro-Na}]^+$ (distributions normalized to n). For $n = 9$ there are three and six molecules on the sides with no Na ($\mathbf{z < 0}$) and one Na ($\mathbf{z > 0}$), respectively. (b) Probability density, as a function of the coordinates of the coronene plane, (x, y), for the $n = 4$ cluster on the $\mathbf{z > 0}$ side, with contour lines superimposed to a cartoon of $[H\text{-coro-Na}]^+$. (c) As in (b), for the three molecules of the $n = 9$ cluster placed on the $\mathbf{z < 0}$ side. (d) As in (b), for the six molecules of the $n = 9$ cluster placed on the $\mathbf{z > 0}$ side: five around the Na atom and the sixth one above it. (For interpretation of the references to color in this figure legend, the reader is referred to the web version of this article.)

the $(H_2)_n[H\text{-coro-Na}]^+$ clusters, defined as $g_c = 100\, n\, m_{H_2}/(n\, m_{H_2} + m_{subs})$, where m_{H_2} and m_{subs} are the masses of H_2 and the substrate, respectively. We have obtained 2.4 wt% and 5.3 wt% for the clusters with $n = 4$ and 9 magic numbers, respectively. The latter is close to the DOE requirement for 2025 [72]. It would be much more adequate to obtain this capacity as a function of temperature and pressure, a goal that can be achieved by means of various methods such as grand canonical Monte Carlo, molecular dynamics or several other thermodynamical calculations [28–30], which however are beyond the scope of the present work. Here, it is interesting to mention recent *ab initio* molecular dynamics simulations of the single-side adsorption to $[coro\text{-Na}]^+$, where gravimetric capacities of 3.0 and 2.4 wt% were found for 77 and 300 K, respectively [44].

5. Conclusion

Clusters of hydrogen molecules adsorbed to bare and sodium-decorated protonated coronene have been studied both experimental and theoretically, with the aim of determining the role played by the alkali atom decoration in the attachment of these molecules to these substrates. The substrates have been produced within multiply charged helium nanodroplets and, after collisions with hydrogen molecules within an RF hexapole evaporation cell, abundances of the resulting clusters, $(H_2)_n[H\text{-coronene-Na}]^+$ and $(H_2)_n[H\text{-coronene}]^+$ have been accurately determined by mass spectrometry. It is found that both bare and decorated supports adsorb similar amounts of hydrogen at the lowest pressures in the H_2 chamber; however, as the pressure increases, the percentage of hydrogen attached to the Na-decorated support steadily increases, reaching about 90% at the highest pressure applied. In addition, some clusters with specific numbers of H_2 molecules attached have been found to be particularly stable, as their abundances were consistently higher than those of neighboring cluster sizes.

On the theoretical side, Diffusion Monte Carlo calculations of these clusters were carried out to obtain their evaporation energies, defined as the minimum energy needed to remove a H_2 molecule from them. The calculations used an Improved Lennard Jones formulation to represent the interactions among the H_2 molecules and the substrates, whose parameters were ultimately determined from the comparison with electronic structure predictions. From the analysis of the evaporation energies of decorated vs. bare supports, we have found a qualitative interpretation of the observed increase of H_2 adsorption by the Na-decorated substrate. Finally, a rather good agreement has been reached regarding the clusters that were found to be stable experimentally and those that exhibit relatively large evaporation energies in the calculations.

The effect on the hydrogen adsorption of decorating coronene with more than one alkali atom, or of producing clusters containing several coronene molecules, could be suitably studied upon slight modifications of the experimental conditions. In addition, it would be of interest to consider larger polycyclic aromatic hydrocarbons, such as circumcoronene and circumcircumcoronene, to investigate how the hydrogen adsorption properties evolve as the prototypes become closer to graphene. Besides hydrogen storage, another interesting application of metal-decorated carbonaceous substrates is the separation of deuterium or tritium isotopologues from a mixture with the most abundant H_2, by exploiting the differences in their adsorption energies [65,80,81]. Work on some of these directions is in progress.

CRediT authorship contribution statement

Esther García-Arroyo: Writing – original draft, Visualization, Investigation, Formal analysis, Data curation. **Anna Maria Reider:** Writing – review & editing, Writing – original draft, Supervision, Investigation, Formal analysis, Data curation. **Siegfried Kollotzek:** Methodology, Investigation, Data curation. **Florian Foitzik:** Visualization, Investigation, Data curation. **José Campos-Martínez:** Writing – review & editing, Formal analysis, Data curation, Conceptualization. **Massimiliano Bartolomei:** Writing – review & editing, Supervision, Methodology, Formal analysis, Data curation, Conceptualization. **Fernando Pirani:** Writing – review & editing, Methodology, Formal analysis. **Marta I. Hernández:** Writing – review & editing, Writing – original draft, Visualization, Formal analysis, Conceptualization. **Massimo Mella:** Writing – review & editing, Writing – original draft, Supervision, Methodology, Conceptualization. **Paul Scheier:** Writing – review & editing, Validation, Formal analysis, Conceptualization.

Declaration of competing interest

The authors declare that they have no known competing financial interests or personal relationships that could have appeared to influence the work reported in this paper.

Acknowledgments

E. García Arroyo is at the Doctoral Programme in Condensed Matter Physics, Nanoscience and Biophysics, Doctoral School Universidad Autónoma de Madrid, Spain. She thanks the iMOVE23 program from CSIC for allowing her a research stay in the University degli Studi dell'Insubria. This work was supported by the Austrian Science Fund, FWF, Grant-DOI 10.55776/P34563 and Grant-DOI 10.55776/W1259, the Spanish Agencia Estatal de Investigación PID2020-114957GB-I00/-AEI/10.13039/501100011033 and PID2020-114654GB-I00/AEI/10.-13039/501100011033, and the Italian Fondo d'Ateneo per la Ricerca. COST Action CA21101 (COSY) and allocation of computing time by CESGA (Spain) are also acknowledged.

Appendix A. Supplementary data

Supplementary material related to this article can be found online at https://doi.org/10.1016/j.ijhydene.2024.07.425.

References

[1] Ren J, Musyoka NM, Langmi HW, Mathe M, Liao S. Current research trends and perspectives on materials-based hydrogen storage solutions: A critical review. Int J Hydrog Energy 2017;42:289–311.

[2] Kojima Y. Hydrogen storage materials for hydrogen and energy carriers. Int J Hydrog Energy 2019;44:18179–92.

[3] Abe J, Popoola A, Ajenifuja E, Popoola O. Hydrogen energy, economy and storage: Review and recommendation. Int J Hydrog Energy 2019;44:15072–86.

[4] Epelle EI, Desongu KS, Obande W, Adeleke AA, Ikubanni PP, Okolie JA, et al. A comprehensive review of hydrogen production and storage: A focus on the role of nanomaterials. Int J Hydrog Energy 2022;47:20398–431.

[5] Zhang L, Allendorf MD, Balderas-Xicohténcatl R, Broom DP, Fanourgakis GS, Froudakis GE, et al. Fundamentals of hydrogen storage in nanoporous materials. Prog Energy 2022;4:042013.

[6] Faye O, Szpunar J, Eduok U. A critical review on the current technologies for the generation, storage, and transportation of hydrogen. Int J Hydrog Energy 2022;47:13771–802.

[7] Bosu S, Rajamohan N. Recent advancements in hydrogen storage - comparative review on methods, operating conditions and challenges. Int J Hydrog Energy 2024;52:352–70.

[8] Ghotia S, Rimza T, Singh S, Dwivedi N, Srivastava AK, Kumar P. Hetero-atom doped graphene for marvellous hydrogen storage: unveiling recent advances and future pathways. J Mater Chem A 2024;12:12325–57.

[9] Patchkovskii S, Tse JS, Yurchenko SN, Zhechkov L, Heine T, Seifert G. Graphene nanostructures as tunable storage media for molecular hydrogen. Proc Natl Acad Sci USA 2005;102:10439–44.

[10] Tozzini V, Pellegrini V. Prospects for hydrogen storage in graphene. Phys Chem Chem Phys 2013;15:80–9.

[11] Mohan M, Sharma VK, Kumar EA, Gayathri V. Hydrogen storage in carbon materials-A review. Energy Storage 2019;1:e35.

[12] Jain V, Kandasubramanian B. Functionalized graphene materials for hydrogen storage. J Mater Sci 2020;55:1865–903.

[13] Bartolomei M, de Tudela RP, Arteaga K, González-Lezana T, Hernández MI, Campos-Martínez J, et al. Adsorption of molecular hydrogen on coronene with a new potential energy surface. Phys Chem Chem Phys 2017;19:26358–68.

[14] Cabria I, López MJ, Alonso JA. Enhancement of hydrogen physisorption on graphene and carbon nanotubes by Li doping. J Chem Phys 2005;123:204721.

[15] Sun Q, Jena P, Wang Q, Marquez M. First-principles study of hydrogen storage on $Li_{12}C_{60}$. J Am Chem Soc 2006;128:9741–5.

[16] Lochan RC, Head-Gordon M. Computational studies of molecular hydrogen binding affinities: The role of dispersion forces,electrostatics, and orbital interactions. Phys Chem Chem Phys 2006;8:1357–70.

[17] Umadevi D, Sastry GN. Molecular and ionic interaction with graphene nanoflakes: a computational investigation of CO_2, H_2O, Li, Mg, Li^+ and Mg^{2+} interaction with polycyclic aromatic hydrocarbons. J Phys Chem C 2011;115:9656–67.

[18] Tachikawa H, Iyama T. Mechanism of hydrogen storage in the graphene nanoflake-lithium-h_2 system. J Phys Chem C 2019;123:8709–16.

[19] Dryza V, Poad B, Bieske E. Attaching molecular hydrogen to metal cations: Perspectives from gas-phase infrared spectroscopy. Phys Chem Chem Phys 2012;14:14954–65.

[20] Du A, Zhu Z, Smith SC. Multifunctional porous graphene for nanoelectronics and hydrogen storage: New properties revealed by first principle calculations. J Am Chem Soc 2010;132:2876–7.

[21] Chen P, Wu X, Lin J, Tan KL. High H_2 uptake by alkali-doped carbon nanotubes under ambient pressure and moderate temperatures. Science 1999;285:91–3.

[22] Mauron P, Remhof A, Bliersbach A, Borgschulte A, Züttel A, Sheptyakov D, et al. Reversible hydrogen absorption in sodium intercalated fullerenes. Int J Hydrog Energy 2012;37:14307–14.

[23] Teprovich JAJ, Wellons MS, Lascola R, Hwang S-J, Ward PA, Compton RN, et al. Synthesis and characterization of a lithium-doped fullerane ($Li_x - C_{60} - H_y$) for reversible hydrogen storage. Nano Lett 2012;12:582–9.

[24] Chen L, Zhang Y, Koratkar N, Jena P, Nayak SK. First-principles study of interaction of molecular hydrogen with li-doped carbon nanotube peapod structures. Phys Rev B 2008;77:033405.

[25] Zhou W, Zhou J, Shen J, Ouyang C, Shi S. First-principles study of high-capacity hydrogen storage on graphene with Li atoms. J Phys Chem Solids 2012;73:245–51.

[26] Seenithurai S, Pandyan RK, Kumar SV, Saranya C, Mahendran M. Li-decorated double vacancy graphene for hydrogen storage application: a first principles study. Int J Hydrog Energy 2014;39:11016–26.

[27] Cabria I, López M, Alonso J. Searching for DFT-based methods that include dispersion interactions to calculate the physisorption of H_2 on benzene and graphene. J Chem Phys 2017;146.

[28] Cabria I. Comparison of theoretical methods of the hydrogen storage capacities of nanoporous carbons. Int J Hydrog Energy 2021;46:12192–205.

[29] Sahoo RK, Chakraborty B, Sahu S. Reversible hydrogen storage on alkali metal (Li and Na) decorated C_{20} fullerene: a density functional study. Int J Hydrog Energy 2021;46:40251–61.

[30] Anikina E, Naqvi SR, Bae H, Lee H, Luo W, Ahuja R, et al. High-capacity reversible hydrogen storage properties of metal-decorated nitrogenated holey graphenes. Int J Hydrog Energy 2022;47:10654–64.

[31] Mahamiya V, Shukla A, Chakraborty B. Potential reversible hydrogen storage in Li-decorated carbon allotrope PAI-graphene: A first-principles study. Int J Hydrog Energy 2023;48:37898–907.

[32] Panella B, Hirscher M, Roth S. Hydrogen adsorption in different carbon nanostructures. Carbon 2005;43:2209–14.

[33] Lovell A, Fernandez-Alonso F, Skipper NT, Refson K, Bennington SM, Parker SF. Quantum delocalization of molecular hydrogen in alkali-graphite intercalates. Phys Rev Lett 2008;101:126101.

[34] Zhou C, Szpunar JA. Hydrogen storage performance in Pd/graphene nanocomposites. ACS Appl Mater Interfaces 2016;8:25933–40.

[35] Kaiser A, Renzler M, Kranabetter L, Schwärzler M, Parajuli R, Echt O, et al. On enhanced hydrogen adsorption on alkali (cesium) doped C_{60} and effects of the quantum nature of the H_2 molecule on physisorption energies. Int J Hydrog Energy 2017;42:3078–86.

[36] Ustinov E, Tanaka H, Miyahara M. Low-temperature hydrogen-graphite system revisited: Experimental study and Monte Carlo simulation. J Chem Phys 2019;151:024704.

[37] Gaboardi M, Pratt F, Milanese C, Taylor J, Siegel J, Fernandez-Alonso F. The interaction of hydrogen with corannulene, a promising new platform for energy storage. Carbon 2019;155:432–7.

[38] Srinivasu K, Chandrakumar KRS, Ghosh SK. Computational investigation of hydrogen adsorption by alkali-metal-doped organic molecules: Role of aromaticity. Chem Phys Chem 2009;10:427–35.

[39] Calvo F, Yurtsever E. Solvation of carbonaceous molecules by para-H_2 and ortho-D_2 clusters. I. Polycyclic aromatic hydrocarbons. J Chem Phys 2016;144:224302.

[40] Goulart M, Kuhn M, Rasul B, Postler J, Gatchell M, Zettergren H, et al. The structure of coronene cluster ions inferred from H_2 uptake in the gas phase. Phys Chem Chem Phys 2017;19:27968–73.

[41] Ghosh A, Debnath T, Ash T, Das AK. Multiple Li^+- and Mg^{2+}-decorated PAHs: potential systems for reversible hydrogen storage. RSC Adv 2017;7:9521–33.

[42] Tachikawa H, Yi H, Iyama T, Yamasaki S, Azumi K. Hydrogen storage mechanism in sodium-based graphene nanoflakes: A density functional theory study. Hydrogen 2022;3:43–52.

[43] Bergmeister S, Kollotzek S, Calvo F, Gruber E, Zappa F, Scheier P, et al. Adsorption of helium and hydrogen on triphenylene and 1 3, 5-triphenylbenzene. Molecules 2022;27:4937.

[44] Petrushenko I, Petrushenko K. Alkali cations and H_2 molecules on BN-doped carbon nanoflakes: Theoretical study. Diam Relat Mater 2023;137:110162.

[45] Jensen PA, Leccese M, Simonsen FDS, Skov AW, Bonfanti M, Thrower JD, et al. Identification of stable configurations in the superhydrogenation sequence of polycyclic aromatic hydrocarbon molecules. Mon Not R Astron Soc 2019;486:5492–8.

[46] Reider AM, Kollotzek S, Scheier P, Calvo F, Yurtsever E, Pirani F, et al. Experimental and theoretical assessment of the enhanced hydrogen adsorption on polycyclic aromatic hydrocarbons upon decoration with alkali metals. Int J Hydrog Energy 2024;58:525–35.

[47] Podeszwa R. Interactions of graphene sheets deduced from properties of polycyclic aromatic hydrocarbons. J Chem Phys 2010;132:044704.

[48] Bartolomei M, Carmona-Novillo E, Hernández MI, Campos-Martínez J, Pirani F. Global potentials for the interaction between rare gases and graphene-based surfaces: An atom-bond pairwise additive representation. J Phys Chem C 2013;117:10512–22.

[49] Lindoy LP, Kolmann SJ, D'Arcy JH, Crittenden DL, Jordan MJ. Path integral Monte Carlo simulations of H_2 adsorbed to lithium-doped benzene: A model for hydrogen storage materials. J Chem Phys 2015;143.

[50] Calvo F, Yurtsever E. Solvation of coronene oligomers by para-H_2 molecules: The effects of size and shape. Phys Chem Chem Phys 2020;22:12465–75.

[51] Tiefenthaler L, Ameixa J, Martini P, Albertini S, Ballauf L, Zankl M, et al. An intense source for cold cluster ions of a specific composition. Rev Sci Instrum 2020;91:033315.

[52] Tiefenthaler L, Kollotzek S, Ellis AM, Scheier P, Echt O. Proton transfer at subkelvin temperatures. Phys Chem Chem Phys 2020;22:28165–72.

[53] Laimer F, Kranabetter L, Tiefenthaler L, Albertini S, Zappa F, Ellis AM, et al. Highly charged droplets of superfluid helium. Phys Rev Lett 2019;123:165301.

[54] García-Arroyo E, Campos-Martínez J, Bartolomei M, Hernández MI, Pirani F, Halberstadt N. Attachment of hydrogen molecules to atomic ions (Na^+ Cl^-): Examination of an adiabatic separation of the H_2 rotational motion. Chem Phys Chem 2023;24:e202300424.

[55] Stephens PJ, Devlin FJ, Chabalowski CF, Frisch MJ. Ab initio calculation of vibrational absorption and circular dichroism spectra using density functional force fields. J Phys Chem 1994;98:11623–7.
[56] Grimme S, Antony J, Ehrlich S, Krieg H. A consistent and accurate ab initio parametrization of density functional dispersion correction (DFT-D) for the 94 elements H-Pu. J Chem Phys 2010;132:154104.
[57] Kendall RA, Dunning J, Thom H, Harrison RJ. Electron affinities of the first-row atoms revisited. Systematic basis sets and wave functions. J Chem Phys 1992;96:6796–806.
[58] Halkier A, Helgaker T, Jørgensen P, Klopper W, Olsen J. Basis-set convergence of the energy in molecular hartree–fock calculations. Chem Phys Lett 1999;302:437–46.
[59] Halkier A, Helgaker T, Jørgensen P, Klopper W, Koch H, Olsen J, et al. Basis-set convergence in correlated calculations on Ne, N_2, and H_2O. Chem Phys Lett 1998;286:243–52.
[60] Grimme S. Improved second-order Møller–Plesset perturbation theory by separate scaling of parallel- and antiparallel-spin pair correlation energies. J Chem Phys 2003;118:9095–102.
[61] Boys SF, Bernardi F. The calculation of small molecular interactions by the differences of separate total energies. some procedures with reduced errors. Mol Phys 1970;19:553–66.
[62] Werner HJ, Knowles PJ, Lindh R, Manby FR, Schütz M, et al. Molpro, version 2022.2, a package of ab initio programs. 2022, See http://www.molpro.net/.
[63] Pirani F, Brizi S, Roncaratti L, Casavecchia P, Cappelletti D, Vecchiocattivi F. Beyond the Lennard-Jones model: A simple and accurate potential function probed by high resolution scattering data useful for molecular dynamics simulations. Phys Chem Chem Phys 2008;10:5489–503.
[64] Ortiz de Zárate J, Bartolomei M, González-Lezana T, Campos-Martínez J, Hernández MI, Pérez de Tudela R, et al. Snowball formation for Cs^+ solvation in molecular hydrogen and deuterium. Phys Chem Chem Phys 2019;21:15662–8.
[65] Mella M, Curotto E. Quest for inexpensive hydrogen isotopic fractionation: Do we need 2D quantum confining in porous materials or are rough surfaces enough? the case of ammonia nanoclusters. J Phys Chem A 2016;120:8148–59.
[66] Mella M, Morosi G, Bressanini D. Time step bias improvement in diffusion Monte Carlo simulations. Phys Rev E 2000;61:2050–7.
[67] Mella M. Higher order diffusion Monte Carlo propagators for linear rotors as diffusion on a sphere: Development and application to $O_2@He_n$. J Chem Phys 2011;135:114504.
[68] Mella M, Curotto E. Assessment of the effects of anisotropic interactions among hydrogen molecules and their isotopologues: A diffusion Monte Carlo investigation of gas phase and adsorbed clusters. J Phys Chem A 2017;121:5005–17.
[69] Håkansson P, Mella M. Improved diffusion Monte Carlo for bosonic systems using time-step extrapolation on the fly. J Chem Phys 2007;126:104106.
[70] Curotto E, Mella M. Diffusion Monte Carlo simulations of gas phase and adsorbed D_2-$(H_2)_n$ clusters. J Chem Phys 2018;148:102315.
[71] Ralser S, Postler J, Harnisch M, Ellis AM, Scheier P. Extracting cluster distributions from mass spectra: Isotopefit. Int J Mass Spectrom 2015;379:194–9.
[72] DOE technical targets for onboard hydrogen storage for light-duty vehicles. 2024, https://www.energy.gov/eere/fuelcells/doe-technical-targets-onboard-hydrogen-storage-light-duty-vehicles. [Accessed 1 July 2024].
[73] Leidlmair C, Wang Y, Bartl P, Schöbel H, Denifl S, Probst M, et al. Structures, energetics, and dynamics of helium adsorbed on isolated fullerene ions. Phys Rev Lett 2012;108:076101.
[74] Kollotzek S, Campos-Martínez J, Bartolomei M, Pirani F, Tiefenthaler L, Hernández MI, et al. Helium nanodroplets as an efficient tool to investigate hydrogen attachment to alkali cations. Phys Chem Chem Phys 2023;25:462–70.
[75] An der Lan L, Bartl P, Leidlmair C, Jochum R, Denifl S, Echt O, et al. Solvation of Na^+, K^+, and their dimers in helium. Chem Eur J 2012;18:4411–8.
[76] González-Lezana T, Echt O, Gatchell M, Bartolomei M, Campos-Martínez J, Scheier P. Solvation of ions in helium. Int Rev Phys Chem 2020;39:465–516.
[77] Prasalovich S, Hansen K, Kjellberg M, Popok V, Campbell EE. Surface entropy of rare-gas clusters. J Chem Phys 2005;123.
[78] Müller S, Mudrich M, Stienkemeier F. Alkali-helium snowball complexes formed on helium nanodroplets. J Chem Phys 2009;131:044319.
[79] Rodríguez-Cantano R, Bartolomei M, Hernández MI, Campos-Martínez J, González-Lezana T, Villarreal P, et al. Comparative investigation of pure and mixed rare gas atoms on coronene molecules. J Chem Phys 2017;146:034302.
[80] Kim JY, Oh H, Moon HR. Hydrogen isotope separation in confined nanospaces: Carbons, zeolites, metal–organic frameworks, and covalent organic frameworks. Adv Mat 2019;31:1805293.
[81] Puricelli S, Bruno G, Gatti C, Ponti A, Mella M. Viability of hydrogen isotopes separation via heterolytic dissociation–driven chemical affinity quantum sieving on inexpensive alkali–earth oxides. Appl Surf Sci 2024;159596.